Visual study of flow patterns during evaporation and condensation of R-600a inside horizontal smooth and helically dimpled tubes

Article (Accepted Version)

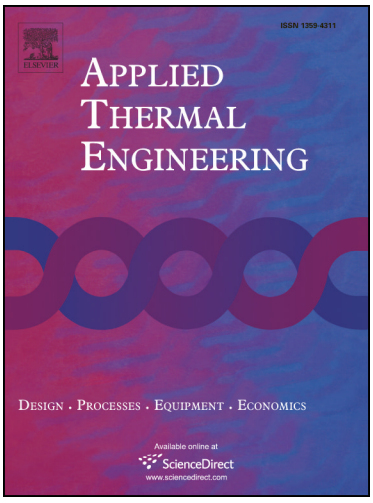

Visual study of flow patterns during evaporation and condensation of R-600a inside horizontal smooth and helically dimpled tubes

H. Mashouf, M. Shafaee, A. Sarmadian, S.G. Mohseni

PII: S1359-4311(17)30974-2
DOI: http://dx.doi.org/10.1016/j.applthermaleng.2017.06.125
Reference: ATE 10644

To appear in: *Applied Thermal Engineering*

Received Date: 19 February 2017
Revised Date: 3 June 2017
Accepted Date: 24 June 2017

Please cite this article as: H. Mashouf, M. Shafaee, A. Sarmadian, S.G. Mohseni, Visual study of flow patterns during evaporation and condensation of R-600a inside horizontal smooth and helically dimpled tubes, *Applied Thermal Engineering* (2017), doi: http://dx.doi.org/10.1016/j.applthermaleng.2017.06.125

Visual study of flow patterns during evaporation and condensation of R-600a inside horizontal smooth and helically dimpled tubes

H. Mashouf[a], M. Shafaee[*,a], A. Sarmadian[a], S.G. Mohseni[b]
[a]Faculty of New Sciences and Technologies, University of Tehran, Tehran, Iran
[b]Energy Institute of Higher Education, Saveh, Iran.
*Corresponding Author, Email: mshafaee@ut.ac.ir, Tel.: +98-919-0110200; fax: +98-21-88497324

ABSTRACT

In this paper, flow patterns and their transitions for the refrigerant R-600a during flow boiling and condensation inside a helically dimpled tube and a smooth tube were observed and analysed. The inner surface of the helically dimpled tube was enhanced by a modified pattern consisting of both shallow and deep protrusions.

For evaporation, the experiments were performed for refrigerant mass velocities in a range of

155 kg/m^{2}s to 467 kg/m^{2}s, all at an average saturation temperature of 56.5℃ with the vapour qualities up to 0.8. Stratified-wavy, intermittent, and annular flows were observed for the smooth tube; for the dimpled tube, the stratified-wavy flow was not seen.

For condensation, all tests were conducted at vapour qualities up to 0.8, and average saturation temperatures ranging between 38℃ and 42℃. The refrigerant mass fluxes varied in the range of 114–368 kg/m^{2}s. Annular, intermittent, and stratified-wavy flows were recognized for the plain tube, but there was no stratified-wavy flow in the flow pattern visualization of the dimpled tube.

The investigation clearly shows that the dimples in both evaporation and condensation have a significant impact on the two-phase flow pattern. Inside the helically dimpled tube, the transition from intermittent to annular (or vice versa) occurred at a lower vapour quality value than for the smooth tube.

Keywords: *Flow pattern; Dimpled tube; R-600a; Evaporation; Condensation.*

1. Introduction

The flow regime characterization is considered one of the most common approaches to describe evaporation and condensation since flow patterns and transport rates between the phases are mutually related. In fact, inside horizontal tubes, the two-phase flow may be dominated by vapour shear or gravity forces. For instance, stratifying-wavy and intermittent flows appear when gravity is the controlling force, while the annular flow pattern is associated with high vapour shear. The effect of the flow regime corresponding to the related mass velocities, vapour qualities, and saturation conditions has a significant influence on the most outstanding models

for the evaluation of local heat transfer coefficients in both evaporation and condensation. Therefore, in order to design a high-performance evaporator and condenser, knowing the flow pattern transitions, as well as their impacts on flow boiling and condensation, can be found worthy of attention.

In recent years, however, it has become common to enhance condensation and evaporation heat transfer inside horizontal tubes by employing surface roughness. Surface-enhanced tubes are widely used especially in the air-conditioning and refrigeration industries, where the benefit of the improved performance overcomes the drawback of the major cost. Actually, that is why they have a noticeable effect on enhancing heat transfer for both evaporation and condensation without introducing excessive penalization in the pressure drop. In this regard, several passive techniques, such as rough surfaces and dimples, have been reviewed by Liu and Sakr [1]. Moreover, Gupta and Uniyal [2] reported that the use of dimples over the heat-exchanger tube surface can be very advantageous in relation to other enhancement methods due to the simplicity of their manufacturing process and as no extra cost is incurred for raw material or labour. Recently, Li et al. appraised the relationship between heat transfer enhancement and the surface geometry of a dimpled enhanced tube using experimental and numerical simulation techniques [3]. Numerical simulations were conducted to simulate the geometric design optimization of enhanced tubes and were validated with experimental data [4]. The results showed that dimples on the tube surface present high heat transfer performance and, compared to the staggered configuration, the inline arrangement of the dimples provided better overall heat transfer characteristics. In addition, the geometric parameters like the shape of the dimple, depth, pitch, and starts were found to have significant effects on the overall heat transfer performance, while the dimple diameter has an insignificant effect on the thermal performance.

In the present study, the advantages of the modified helically dimpled pattern based on the application of both deep and shallow dimples are the basic concepts of the dimpled tube design. The dimpled tube concept means reshaping the plain tube, so that evenly placed dimples (deep and shallow ones) form in the tube wall. At first, it can lead to the creation of swirling in the flow in areas close to the wall; eventually, it can produce the separation of flow. On the other hand, it can produce a surface area increase. All of them give rise to increased performance through a combination of increased turbulence, boundary layer disruption, secondary flow generation, increased heat transfer surface area, and more nucleation sites. All of the mentioned factors cause an increase in the heat transfer coefficient.

Recently, in some experimental investigations, the application of dimples on the walls of tubes like shallow square dimples [5], dimple/protrusion and secondary petal arrays which is produced by Vipertex^{TM} and has been named 1EHT tube (experiments of outside [6] and inside [7] condensation and evaporation heat transfer) and EHT tube [8], and both shallow and deep dimples/protrusions during evaporation and condensation of R-600a inside helically dimpled tube in our previous papers [9, 10] show a proper heat transfer augmentation. However, all of them did not perform a flow pattern visualization. In fact, widespread knowledge about flow patterns is available for horizontal smooth tubes in the literature. To discriminate between flow patterns inside horizontal smooth tubes under adiabatic and diabatic conditions, numerous flow pattern maps or criteria for transition between flow patterns have been proposed (El Hajal et al. [11], 2003; Thome et al. [12], 2003; Thome [13], 2003; Kattan et al. [14], 1998a; Olivier et al. [15], 2007; Tandon et al. [16], 1982). However, there is no information about the effect of dimples on flow pattern behaviour. Thus, extensive experimental data is needed to improve the knowledge of the governing phenomena. At the same time, the application of hydrocarbons to

replace conventional refrigerants in refrigeration and air-conditioning systems have been studied due to their zero ozone-depletion potential and negligible global warming potential [17]. For instance, Lee et al., in an experimental study [18], discussed that R-600a has a better energy performance compared to other refrigerants. Moreover, Chao-Chieh Yu and Tun-Ping Teng [19] indicated that the use of R-600a can enhance the enhancement factors (EFs) of refrigerators. Therefore, a visual inspection was carried out to determine the flow patterns for the evaporation and condensation of R-600a inside a dimpled tube with a new enhanced geometry and a plain tube.

2. Experimental details

2.1. Experimental loop

The schematic layout of the test apparatus used for condensation and evaporation is reported in **Fig. 1**. The test apparatus consisted of two main closed loops: the cold-water loop and the refrigerant loop. The cold-water loop was connected to the condensers. Cold water removed the latent heat from the condensing refrigerant. The water temperature was kept constant in the range of 14–16℃. The main components of the refrigerant loop were: needle valves, a variable-frequency gear pump (ZDF, Czech Republic), a Coriolis-effect mass flow meter (MASS/2100/6000, Danfoss, Denmark), pre-evaporators, a test evaporator, sight glasses, a test condenser, a post-condenser, a reservoir, and necessary instruments for measurements and controls.

The refrigerant was injected into the cycle via the needle valve. The gear pump, with variable frequency, preciously adjustable stroke and flow rate, and nominal power of 20 L/min, was

coupled with an inverter. It circulated the refrigerant and controlled the mass velocity. The flow meter was a Coriolis-effect mass flow meter with an accuracy within 0.1% of the full scale.

During the experiments, a short range of vapour qualities was achieved in a single test run. Therefore, two pre-evaporators were used to cover the entire range of vapour qualities. The pre-evaporators were installed just before the test evaporator. The refrigerant reached the saturated condition through the first pre-evaporator. RTD PT100 thermometers with a calibrated accuracy of 0.1℃ and pressure transducers (EN 837-1, Wika) with an accuracy within ±0.1% of the full scale are located at the pre-evaporators' inlets, the test evaporator inlet, and the test condenser inlet to determine the enthalpy of the refrigerant at these inlets. The post-condenser and reservoir were provided in order to reach the steady condition and stabilize the operating condition, as well as to ensure that the refrigerant was liquid before entering the pump and flow meter.

2.2. Test sections

The test condenser was a double-pipe heat exchanger in which the coolant was circulated in the annulus and the refrigerant flowed through the inner tube. The RTD-PT100 thermometers were also installed in the setup to measure cooling water temperatures at the inlet and outlet of the test condenser. The test evaporator and pre-evaporators were heated by three flexible electrical heating tapes of 3 kW capacity with adjustable power. These tapes were wrapped around them and electrically insulated. By regulating the alternating current (AC) voltage as per the electrical coil around the pre-evaporators, the vapour quality at the inlet of the test evaporator was controlled. Both the AC voltage and current had uncertainties of 0.1%. All the evaporators and condensers were thermally insulated with 20-mm-thick glass wool to minimize heat loss through their walls. Two PDM-75 differential pressure-drop transducer apparatus with an

accuracy of 0.075% of the full scale were installed to quantify the pressure drop through the test sections. This apparatus was calibrated to measure the pressure drop in the range of 0–150 kPa. The saturation temperatures at the average pressure of the test sections were considered as the saturation temperatures of the whole test sections.

Two types of tubes were utilized as the test tube for the test evaporator and the test condenser. These were one smooth tube and one newly designed tube that was enhanced by a kind of surface roughness. The parameters of the latter are shown in **Fig. 2**. The dimples were arranged helically with a pitch ratio ($= p/d$) of 1.21 on the test section. The diameters and depths of the shallow dimples were maintained at a constant value of 1 mm and 0.5 mm, respectively. The diameters and depths of the deep dimples were maintained at a constant value of 2 mm and 1 mm, respectively. Both the tubes have an outer diameter of 9.5 mm, a thickness of 0.6 mm, and a length of 1,100 mm.

2.3. Visualization and test procedure

Two sight glasses were mounted at the end of the test evaporator and the test condenser in order to visualize the flow patterns. The sight glasses, which were made of Pyrex glass, had a length of 120 mm and an inner diameter identical to that of the test tube. Notably, flow patterns were observed through the sight glasses, but these had no dimples or protrusions. Taitel and Dukler [20] noted that the phase distribution of the two phases, such as the liquid height in the tube, is mainly influenced by the mass fluxes, vapour mass qualities, thermophysical properties of the working fluids, and shear stress on the tube wall. The wall shear stress is influenced by the wall roughness only when the flow is in the turbulent-roughed flow region [21]. Our experiment covered the turbulent-smooth flow region, which minimized the flow pattern difference between

the glass tube and the copper tube. Therefore, it was assumed that the flow structure should experience only a minor disruption in passing through the glass tube, and the flow should not redevelop significantly through the sight glasses because of its short length.

A diffuse white film pigmented with evenly spaced black stripes was placed behind the sight glass and illuminated. This method was originally developed by Jassim et al. [22]. The black stripes provide a contrast that enhances the image and allows for the detection of fine liquid films. The stripe width, spacing, and distance from the centre line of the test sections were determined as described by Jassim et al. [22].

The tests were performed at selected mass velocities of 467 kg/m^{2}s, 424 kg/m^{2}s, 368 kg/m^{2}s, 307 kg/m^{2}s, 260 kg/m^{2}s, 207 kg/m^{2}s, and 155 kg/m^{2}s for evaporation, and mass velocities of 368 kg/m^{2}s, 270 kg/m^{2}s, 155 kg/m^{2}s, and 114 kg/m^{2}s for condensation. The experiments were conducted at an average saturation temperature of 56.5℃ for the evaporation test and 40℃ for condensation. The range of operating parameters in the present study is given in **Table 1**.

3. Data reduction

The experimental apparatus was installed to visualize the flow patterns inside a smooth and a dimpled tube during condensation and evaporation. It was assumed that the system reached the steady state condition when the temperature and pressure were constant for at least 15 minutes. Then some tests were iterated twice to check the reproducibility of the test apparatus. The data was assembled for the flow of R-600a inside a smooth tube to establish the integrity of the experimental apparatus and to measure its flow pattern against the flow pattern of the dimpled tube. The data for the dimpled tube was collected to establish a flow pattern map.

3.1. Evaporation

The single-phase R-600a flow was performed to obtain the evaporators' efficiencies. The evaporator's thermal efficiency was:

$$\gamma_e = \dot{m}_{ref}(h_2 - h_1)/(VI)_{pe} \quad (1)$$

where $\dot{m}_{ref}$, V, I, h_2, and $h_1$are the refrigerant mass flow rate, the electric voltage, the electric current, the enthalpy of the refrigerant at the pre-evaporator inlet taken at inlet temperature and pressure of the sub-cooled refrigerant, and the enthalpy of the refrigerant at the test evaporator outlet based on the outlet temperature and pressure of the sub-cooled flow, respectively. The measured evaporator thermal efficiency was about 0.95.

The quality of the refrigerant at the inlet (x_{in}) and outlet (x_{out}) of the test evaporator were calculated from the following equations:

$$Q_{t,pe} = \gamma_e(VI)_{pe} = Q_{sen} + Q_{lat} \quad (2)$$

$$Q_{sen} = C_p\dot{m}_{ref}\left(T_{sat,pe} - T_{ref,pe,in}\right) \quad (3)$$

$$Q_{lat} = \dot{m}_{ref}h_{fg,pe}x_{in,te} \quad (4)$$

By substituting Eq. (2) and Eq. (3) in Eq. (4) and rearranging, the inlet quality of the test section can be expressed as:

$$x_{in,te} = \frac{Q_{t,pe} - C_p \dot{m}_{ref}(T_{sat,pe} - T_{ref,pe,in})}{\dot{m}_{ref} h_{fg,pe}} \quad (5)$$

$$x_{out,te} = x_{in,te} + \gamma_e (VI)_{te} / \dot{m}_{ref} h_{fg,te} \quad (6)$$

where:

$Q_{t,pe}$ is the total heat transferred in the pre-evaporator, Q_{sens} is the sensible heat, Q_{lat} is the latent heat, C_p is the specific heat of the refrigerant taken at the average refrigerant temperature through the first pre-evaporator, $T_{sat,pe}$ is the saturated temperature of the refrigerant taken at the average pressure of the first pre-evaporator, $T_{ref,pe,in}$ is the temperature of the refrigerant at the inlet of the pre-evaporator, $h_{fg,pe}$ is the vaporization enthalpy of the refrigerant at the average pressure of the second pre-evaporator, and $h_{fg,te}$ is the vaporization enthalpy of the refrigerant at the average pressure of test evaporator.

3.2. Condensation

Heat leakage from the test condenser was considered by the following equation which was used by Xing et al. [1]:

$$\gamma_c = \frac{\dot{m}_w C_{p,w}(T_{w,out} - T_{w,in})}{\dot{m}_{ref} C_{p,ref}(T_{ref,in} - T_{ref,out})} \quad (7)$$

where $C_{p,w}, \dot{m}_w, T_{w,out},$ and $T_{w,in}$ are the specific heat of water at average water temperature through the annulus, the mass flow rate of water, the annulus outlet temperature of water, and the annulus inlet temperature of water, respectively. The measured γ_{con} reached about 0.97.

For in-tube condensation, the inlet quality of the test condenser was obtained by:

$$x_{in,tc} = (\gamma_e (VI)_e - C_p \dot{m}_{ref}(T_{ref,e,sat} - T_{ref,e,in}))/\dot{m}_{ref} h_{fg,e} \quad (8)$$

where $C_p, T_{sat,e,in}, T_{ref,e,in}$, and $h_{fg,e}$ are the specific heat of the refrigerant taken at the average refrigerant temperature through the pre-evaporators, the saturated temperature of the refrigerant taken at the average pressure of the pre-evaporators, the temperature of the refrigerant at the inlet of the pre-evaporators, and the vaporization enthalpy of the refrigerant at the average pressure of the pre-evaporators, respectively.

The total heat transfer from the test condenser was calculated from an energy balance for the cooling water flowing through the annulus:

$$Q_w = \gamma_c C_{p,w} \dot{m}_w (T_{w,out} - T_{w,in}) \quad (9)$$

where $Q_w, C_{p,w}, \dot{m}_w, T_{w,out}$, and $T_{w,in}$ are the total heat transferred from the test condenser, the specific heat of water at the average water temperature through the annulus, the mass flow rate of water, the annulus outlet temperature of water, and the annulus inlet temperature of water, respectively.

The quality of refrigerant at the outlet of the test condenser $x_{out,tc}$ was calculated from an energy balance on the test condenser:

$$x_{out,tc} = x_{in,tc} - Q_w/(\dot{m}_{ref}.h_{fg,tc}) \quad (10)$$

where $h_{fg,tc}$ is the vaporization enthalpy of the refrigerant at the average pressure of the test condenser.

3.3. Uncertainty analysis

The uncertainty analysis of the results was performed using the method proposed by R. R. Schultz and R. Cole [23]. They suggested the following method for analysing the effect of uncertainty in each variable on the uncertainty of the result:

$$U_R = \left[\sum_{i=1}^{n}\left(\frac{\partial R}{\partial V_i}U_{V_i}\right)^2\right]^{1/2} \tag{11}$$

where U_R is the estimate of the uncertainty in the calculated value of the desired variable R, due to the independent uncertainty U_{V_i}in the primary measurement of n number of variables, V_i, affecting the result. Applying Eq. (11), the uncertainty in the vapour quality calculation for evaporation and condensation can be written as:

$$U_{x_e} = \left\{\left[\frac{2\gamma_{eva}IU_V}{\dot{m}_{ref}h_{fg,pe}}\right]^2 + \left[\frac{2\gamma_{eva}VU_I}{\dot{m}_{ref}h_{fg,pe}}\right]^2 + \left[\frac{2\gamma_{eva}VIU\dot{m}_{ref}}{\dot{m}_{ref}{}^2h_{fg,pe}}\right]^2 + 2\left[\frac{C_pU_T}{h_{fg,pe}}\right]^2\right\}^{1/2} \tag{12}$$

$$U_{x_c} = \left\{\left[\frac{\gamma_eIU_V}{\dot{m}_{ref}h_{fg,e}}\right]^2 + \left[\frac{\gamma_eVU_I}{\dot{m}_{ref}h_{fg,e}}\right]^2 + \left[\frac{\gamma_eVIU\dot{m}_{ref}}{\dot{m}_{ref}{}^2h_{fg,e}}\right]^2 + 2\left[\frac{C_pU_T}{h_{fg,e}}\right]^2 + \left[\frac{\gamma_cC_{p,w}(T_{w,out}-T_{w,in})U\dot{m}_w}{\dot{m}_{ref}h_{fg,e}}\right]^2 + 2\left[\frac{\gamma_cC_{p,w}\dot{m}_wU_{T_w}}{\dot{m}_{ref}h_{fg,e}}\right]^2\right\}^{1/2} \tag{13}$$

It was found that the uncertainty in the determination of vapour quality for evaporation and condensation were about 4.98 per cent and 5.5 per cent for all the test runs, respectively.

4. Results and discussion

The flow pattern visualization aims to compare the behaviour of the smooth tube with that of the helically dimpled tube. This task was performed by taking a photo of the sight glasses with a high-speed photography camera. Then, the photos were compared with the flow pattern

definition available in the literature. To point out the differences between the smooth tube and the dimpled tube in a better way, the data points were thickened close to the transition regions. The results of evaporation and condensation in both the plain and dimpled tubes are discussed in separate sections as follows:

4.1. Evaporation

For the smooth tube, a two-phase flow pattern map proposed by Thome et al. [12] was taken into account. In this format of the flow regime map, the vapour quality x is taken along the abscissa, whereas the mass flux G is taken along the ordinate. Forty-nine data points were collected during the evaporation of R600-a inside the smooth tube. These are represented in **Fig. 3** and compared with the flow pattern map of Thome et al. [12]. The stratified-wavy, intermittent, and annular flow regimes, as well as their transition, were observed during the visualization. As can be seen from **Fig. 3**, the transition from the stratified-wavy to the intermittent regime takes place at higher mass fluxes than those indicated by the map. In addition, the comparison between the data and the boundary between the intermittent and annular flows shows that the map provides a good agreement with those predicted by the map.

Fifty flow pattern data points for the evaporation of R600-a in the helically dimpled tube are reported in **Fig. 4**. Furthermore, the transition lines from stratified-wavy to intermittent and from intermittent to annular for the smooth tube are illustrated too. In order to draw a comparison between the helically dimpled tube and the smooth tube, **Fig. 4** and **Fig. 5** should be considered together. During the experiment, two main flow patterns (intermittent and annular) for the helically dimpled tube were observed, while three main flow regimes (stratified-wavy, intermittent, and annular) were recognized for the smooth tube. As can be seen from **Fig. 5**, the

flow at $x = 0.15$ and the mass flux of 155 kg/m^{2}s for the helically dimpled tube has large-amplitude waves that wash the top of the tube (intermittent flow). In contrast, at $x = 0.15$ and mass flux of 155 kg/m^{2}s for the smooth tube, the two phases flow separately with low waves travelling in the direction of the flow that do not reach the top of the tube (stratified-wavy). The flow at $x = 0.3$ and mass flux of 155 kg/m^{2}s for the helically dimpled tube moves towards the tube wall perimeter and covers the upper region of the tube wall as a thin liquid film, and the inside wall of the tube becomes totally wet, whereas most of the liquid flows in the bottom of the tube surface. The interface of the liquid and gas phase in this flow pattern has a remarkable turbulence. But the flow inside the smooth tube at $x = 0.31$ and mass flux of 155 kg/m^{2}s remains intermittent. The flow at $x = 0.61$ and mass flux of 155 kg/m^{2}s inside the dimpled tube, as well as at $x = 0.78$ and mass flux of 155 kg/m^{2}s for the smooth tube, is annular; however, the liquid film thickness at the bottom of the dimpled tube is thinner than that of the smooth tube. These behaviours are the same for the rest of the mass fluxes. The dimples alter the flow field in a circular tube in several different ways. The blockage and partitioning of the flow cross-section by the finite-thickness of dimples increase the axial velocity and the wetted perimeter. The partitioned, helically twisting duct also provides a longer effective flow path and imposes a curvature-induced transverse force on the axial flow to produce secondary circulation. Considering all the data shown in **Fig. 4** gives rise to two main comments: First, the transition from intermittent to annular flow generally occurs at a lower vapour quality value than for the smooth tube. Second, in the region where the flow is stratified-wavy for the smooth tube, the flow inside the dimpled tube is intermittent. **Fig. 5** also shows that at $x = 0.16$ and mass flux of 424 kg/m^{2}s for the helically dimpled tube, the large radial acceleration induced by dimples causes the bubbles to migrate to the centre of the tube, resulting in rapid condensation of the

vapour. Meanwhile, in the smooth tube, at $x = 0.23$ and mass flux of 424 kg/m^{2}s, the bubbles remain near the heated surface, condensing rather slowly as they are swept downstream.

4.2. Condensation

First, 45 data points were assembled during the condensation of R600-a inside the smooth tube and compared with the flow pattern map that was developed by El Hajal et al. [11], which is shown in **Fig. 6**. Three main flow patterns were observed during the experiments: stratified-wavy, intermittent, and annular. From **Fig. 6**, it can be seen that the transition from stratified-wavy flow to intermittent flow for $x < 0.4$ and the transition from intermittent to annular flow have a good agreement with those predicted by the map.

As can be seen in **Fig. 7**, 36 flow pattern data points relating to the condensation of R600-a inside the helically dimpled tube and the transition line from intermittent to annular flow for the smooth tube are illustrated. The experiments reveal two main flow regimes (intermittent and annular) for the dimpled tube, which is shown in **Fig. 8**(a). From **Fig. 7**, it was observed that the dimples in the helically dimpled tube delay the transition from annular flow to intermittent flow, which can enhance the heat transfer relative to the smooth tube counterpart. By considering **Fig. 8**, it can be observed that the flow inside the dimpled tube at $G = 155$ kg/m^{2}s and $x = 0.19$ experiences intermittent flow, whereas in the smooth tube at $G = 155$ kg/m^{2}s and $x = 0.23$, the stratified-wavy flow prevails. It should be noticed that for condensation, the only difference is that the top of the tube in a stratified-wavy flow will be wetted by film condensation rather than remain dry during evaporation. The flow inside the smooth tube at $x = 0.38$ and mass flux of 155 kg/m^{2}s is intermittent. In contrast, the flow at $x = 0.3$ and mass flux of 155 kg/m^{2}s for the helically dimpled tube moves towards the tube wall perimeter and covers the upper region of the tube wall as a thin liquid film. The interface of the liquid and gas phases in this flow pattern

shows remarkable turbulence. The liquid film thickness at the bottom of the dimpled tube is thinner than that of the smooth tube. These behaviours are the same for the rest of the mass fluxes.

5. Conclusions

Experimental investigations were performed to observe the evaporation and condensation flow patterns of the refrigerant R-600a inside a helically dimpled tube and a smooth tube.

The following conclusions can be highlighted as the main results of the experiments:

a) During the evaporation and condensation of R-600a inside the dimpled tube at experiment conditions, two main flow patterns were observed: intermittent and annular flow. Evaporation and condensation inside the smooth tube at the same condition, however, lead to three main flow patterns: intermittent, annular, and stratified-wavy.

b) In evaporation, it was observed that the dimples in the helically dimpled tube caused the intermittent-annular flow transitions to occur at lower vapour qualities than the smooth tube, which can enhance the heat transfer relative to the smooth tube counterpart.

c) During condensation, the transition from annular to intermittent flow took place at a lower vapour quality value than for the smooth tube. In the region where the flow is stratified-wavy for the smooth tube, the flow inside the dimpled tube is intermittent.

Nomenclature

$\dot{m}$	mass flow rate (kg/s)
A	Annular
d	diameter(mm)
G	mass velocity (kg/m^{2}s)
h	specific enthalpy (kJ/kg)

I	current (A)
I	intermittent
P	pressure (kPa)
Q	rate of heat transfer (W)
q	heat flux (kW/m^2)
S	stratified
S-W	stratified-wavy
T	temperature (K)
V	voltage (V)
x	vapor quality
p	pitch ratio
C_p	specific heat (kJ/kg K)
γ	insulation efficiency

Subscripts

f	liquid phase
g	vapor phase
lat	latent
pe	pre-evaporator
ref	refrigerant
sat	saturated
sen	sensible
t	total
tc	test condenser
te	test evaporator
e	evaporator
c	condenser
w	water
in	inlet
out	outlet

References

[1] S. Liu, M. Sakr, A comprehensive review on passive heat transfer enhancements in pipe exchangers, Renewable and sustainable energy reviews, 19 (2013) 64-81.
[2] A. Gupta, M. Uniyal, Review of heat transfer augmentation through different passive intensifier methods, IOSR Journal of Mechanical and Civil Engineering (IOSRJMCE) ISSN, (2012) 2278-1684.
[3] M. Li, T.S. Khan, E. Al-Hajri, Z.H. Ayub, Single phase heat transfer and pressure drop analysis of a dimpled enhanced tube, Applied Thermal Engineering, 101 (2016) 38-46.
[4] M. Li, T.S. Khan, E. Al Hajri, Z.H. Ayub, Geometric optimization for thermal–hydraulic performance of dimpled enhanced tubes for single phase flow, Applied Thermal Engineering, 103 (2016) 639-650.
[5] I.P. Nascimento, E.C. Garcia, Heat transfer performance enhancement in compact heat exchangers by using shallow square dimples in flat tubes, Applied Thermal Engineering, (2015).
[6] D.J. Kukulka, R. Smith, W. Li, Comparison of condensation and evaporation heat transfer on the outside of smooth and enhanced 1EHT tubes, Applied Thermal Engineering, (2016).

[7] D.J. Kukulka, R. Smith, W. Li, Comparison of tubeside condensation and evaporation characteristics of smooth and enhanced heat transfer 1EHT tubes, Applied Thermal Engineering, (2015).
[8] S.-p. Guo, Z. Wu, W. Li, D. Kukulka, B. Sundén, X.-p. Zhou, J.-j. Wei, T. Simon, Condensation and evaporation heat transfer characteristics in horizontal smooth, herringbone and enhanced surface EHT tubes, International Journal of Heat and Mass Transfer, 85 (2015) 281-291.
[9] M. Shafaee, H. Mashouf, A. Sarmadian, S. Mohseni, Evaporation heat transfer and pressure drop characteristics of R-600a in horizontal smooth and helically dimpled tubes, Applied Thermal Engineering, 107 (2016) 28-36.
[10] A. Sarmadian, M. Shafaee, H. Mashouf, S. Mohseni, Condensation heat transfer and pressure drop characteristics of R-600a in horizontal smooth and helically dimpled tubes, Experimental Thermal and Fluid Science, 86 (2017) 54-62.
[11] J. El Hajal, J.R. Thome, A. Cavallini, Condensation in horizontal tubes, part 1: two-phase flow pattern map, International Journal of Heat and Mass Transfer, 46 (2003) 3349-3363.
[12] J.R. Thome, J.E. Hajal, Two-phase flow pattern map for evaporation in horizontal tubes: latest version, Heat Transfer Engineering, 24 (2003) 3-10.
[13] J. Thome, Update on the Kattan-Thome-Favrat flow boiling model and flow pattern map, in: 5th International Boiling Conference, 2003.
[14] N. Kattan, J. Thome, D. Favrat, Flow boiling in horizontal tubes: Part 1—Development of a diabatic two-phase flow pattern map, Journal of Heat Transfer, 120 (1998) 140-147.
[15] J.A. Olivier, L. Liebenberg, J.R. Thome, J.P. Meyer, Heat transfer, pressure drop, and flow pattern recognition during condensation inside smooth, helical micro-fin, and herringbone tubes, International Journal of Refrigeration, 30 (2007) 609-623.
[16] T. Tandon, H. Varma, C. Gupta, A new flow regimes map for condensation inside horizontal tubes, Journal of Heat Transfer, 104 (1982) 763-768.
[17] A.S. Padalkar, K.V. Mali, S. Devotta, Simulated and experimental performance of split packaged air conditioner using refrigerant HC-290 as a substitute for HCFC-22, Applied Thermal Engineering, 62 (2014) 277-284.
[18] H.-S. Lee, J.-I. Yoon, J.-D. Kim, P. Bansal, Characteristics of condensing and evaporating heat transfer using hydrocarbon refrigerants, Applied Thermal Engineering, 26 (2006) 1054-1062.
[19] C.-C. Yu, T.-P. Teng, Retrofit assessment of refrigerator using hydrocarbon refrigerants, Applied Thermal Engineering, 66 (2014) 507-518.
[20] Y. Taitel, A. Dukler, A model for predicting flow regime transitions in horizontal and near horizontal gas-liquid flow, AIChE Journal, 22 (1976) 47-55.
[21] J. Nikuradse, Laws of flow in rough pipes, National Advisory Committee for Aeronautics Washington, 1950.
[22] E.W. Jassim, T.A. Newell, J.C. Chato, Probabilistic determination of two-phase flow regimes in horizontal tubes utilizing an automated image recognition technique, Experiments in fluids, 42 (2007) 563-573.
[23] R. Schultz, R. Cole, Uncertainty analysis in boiling nucleation, in: AIChE symposium series, Vol. 75, 1979, pp. 32-38.

Figure caption list

Fig. 1 *Schematic diagram of experimental facilities*

Table caption list

Table 1. Ranges of the operating parameters in the present study.

Parameter	Range
Refrigerant	R-600a
Inside diameter	8.25(mm)
Thickness	0.6(mm)
Refrigerant mass velocity (evaporation)	155-467(kg/m^2 s)
Refrigerant mass velocity (condensation)	114-368(kg/m^2 s)
Vapor quality	0-0.8
Average pressure (evaporation)	8 (bar)
Average pressure (condensation)	5.3(bar)

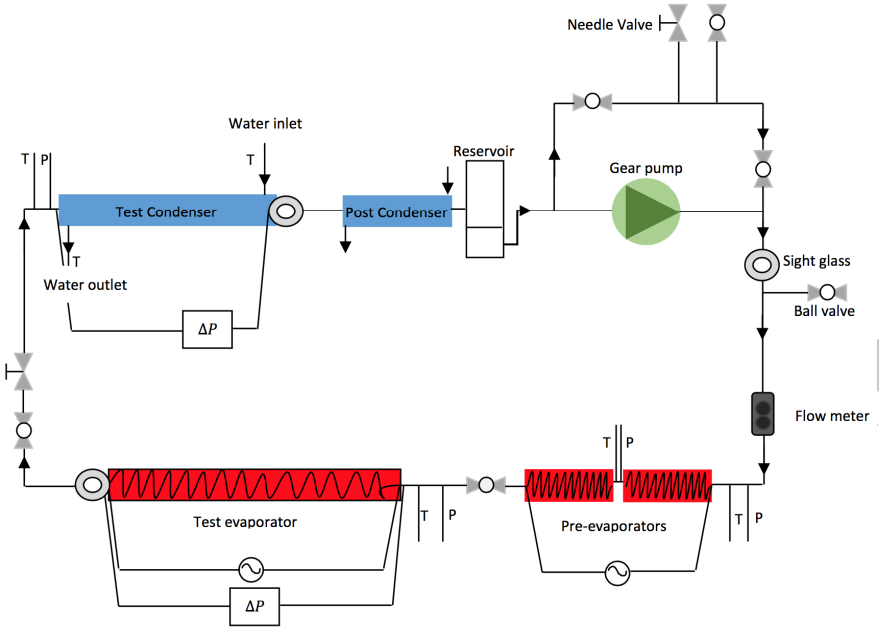

Fig. 1. Schematic diagram of experimental facilities

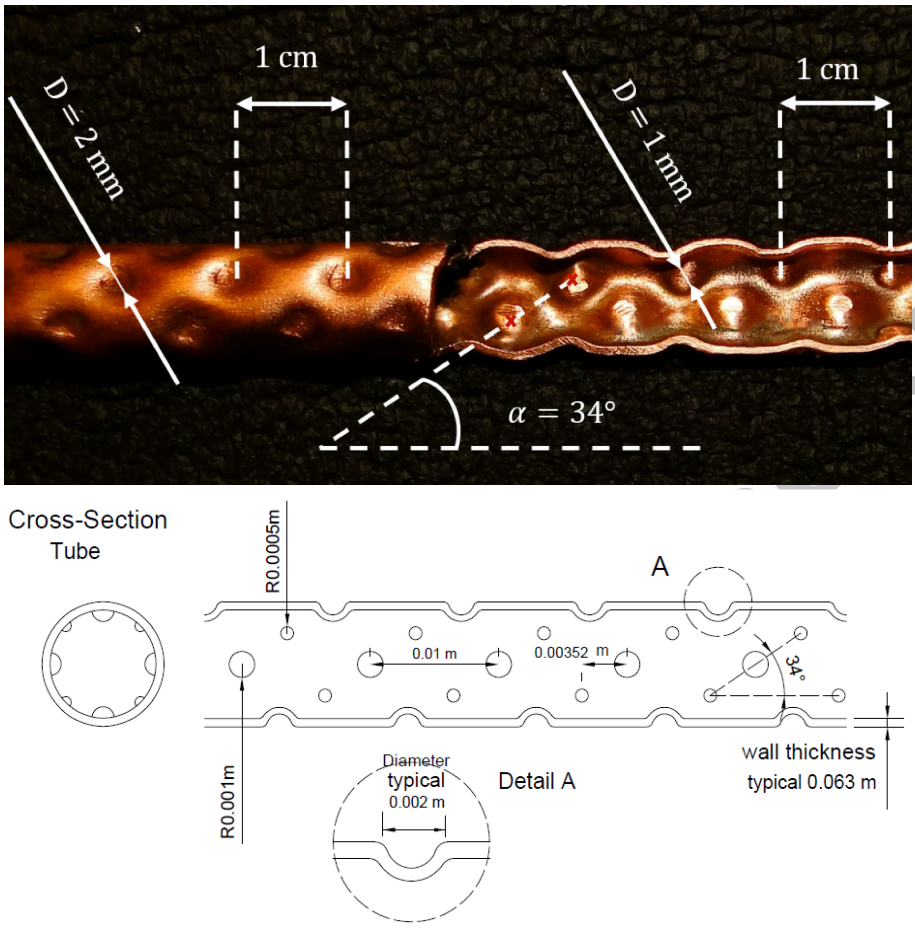

Fig. 2. Helically dimpled tube illustration and its pattern characteristics.

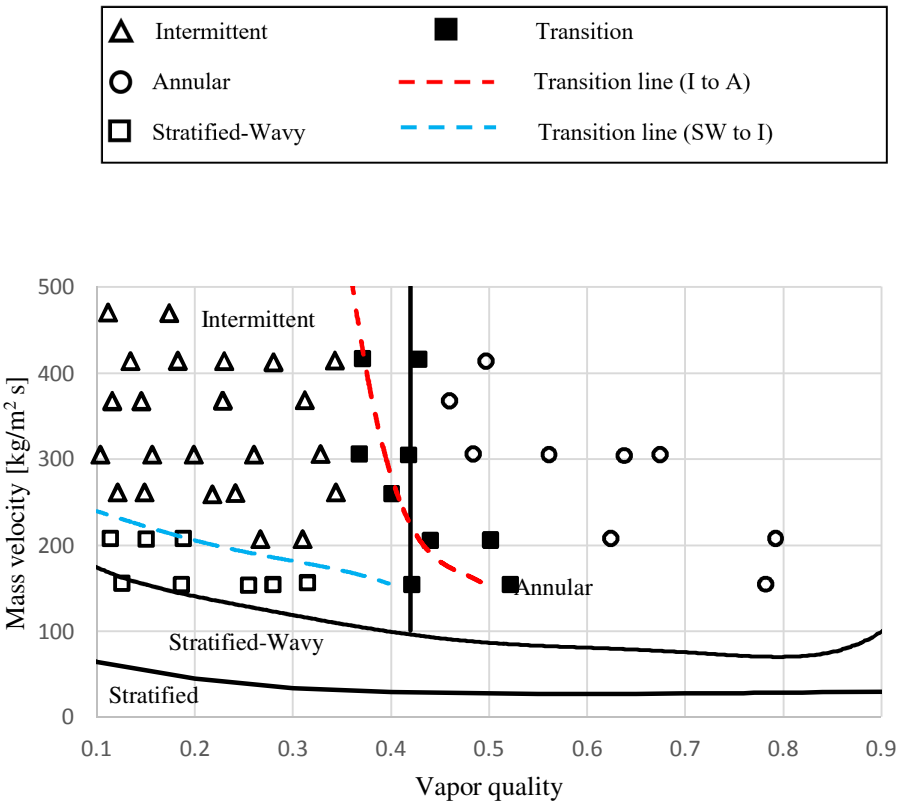

Fig. 3. Comparison between the observed flow patterns for the smooth tube and the Thome et al. [12] map.

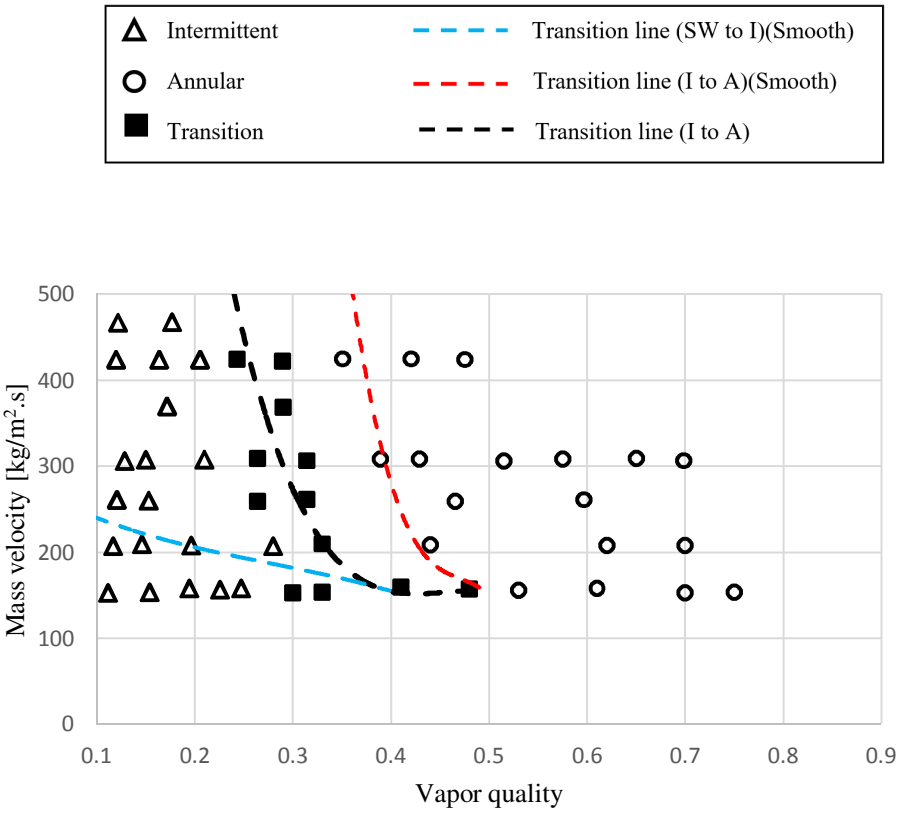

Fig. 4. Observed flow patterns for the helically dimpled tube. Data are reported using the coordinates of the Thome et al. [12] map.

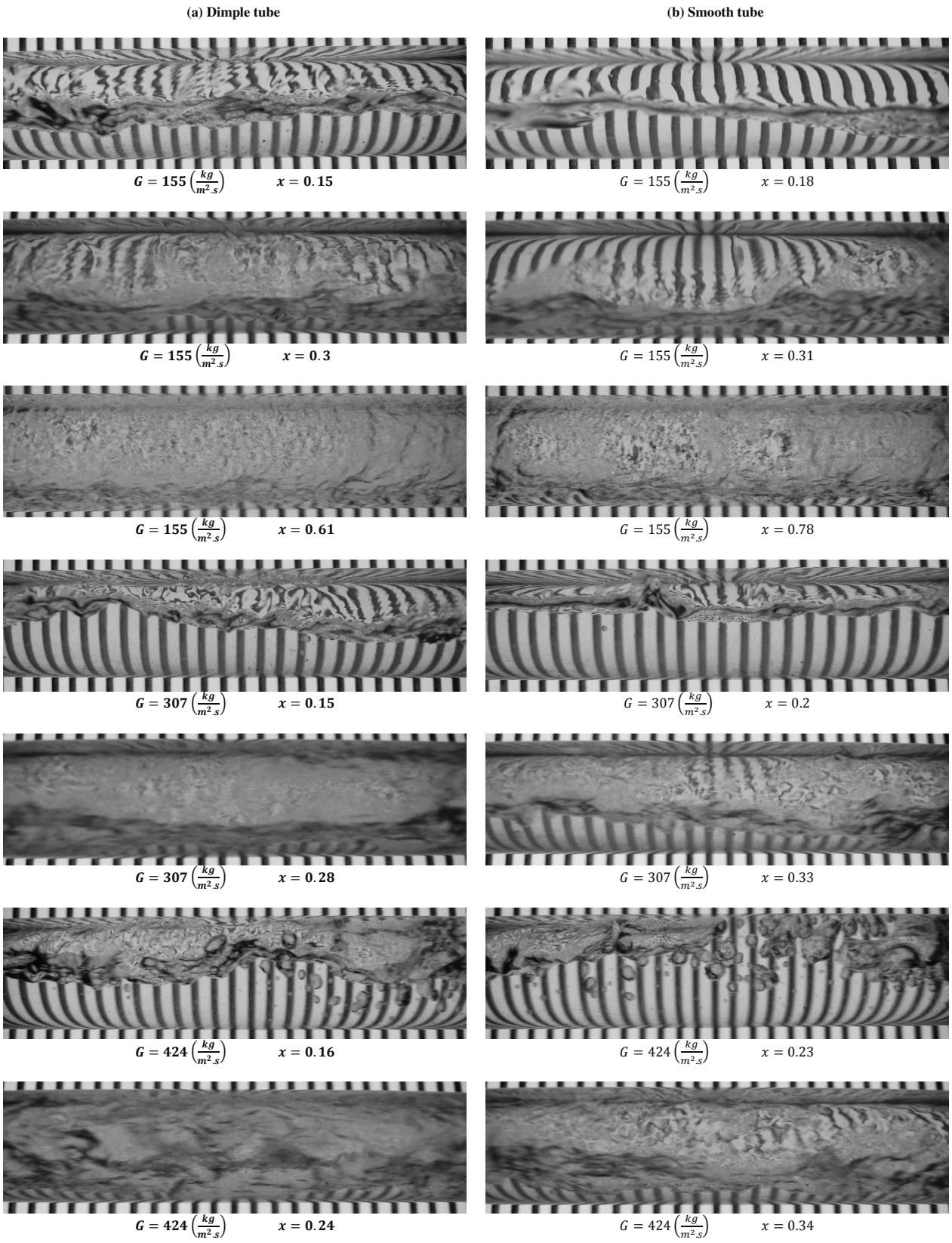

Fig. 5. Two-phase flow patterns for evaporation inside a) helically dimpled tube versus b) plain tube at three mass fluxes of 155 kg m^{-2} s^{-1}, 307 kg m^{-2} s^{-1}, and 424 kg m^{-2} s^{-1} at different vapor qualities.

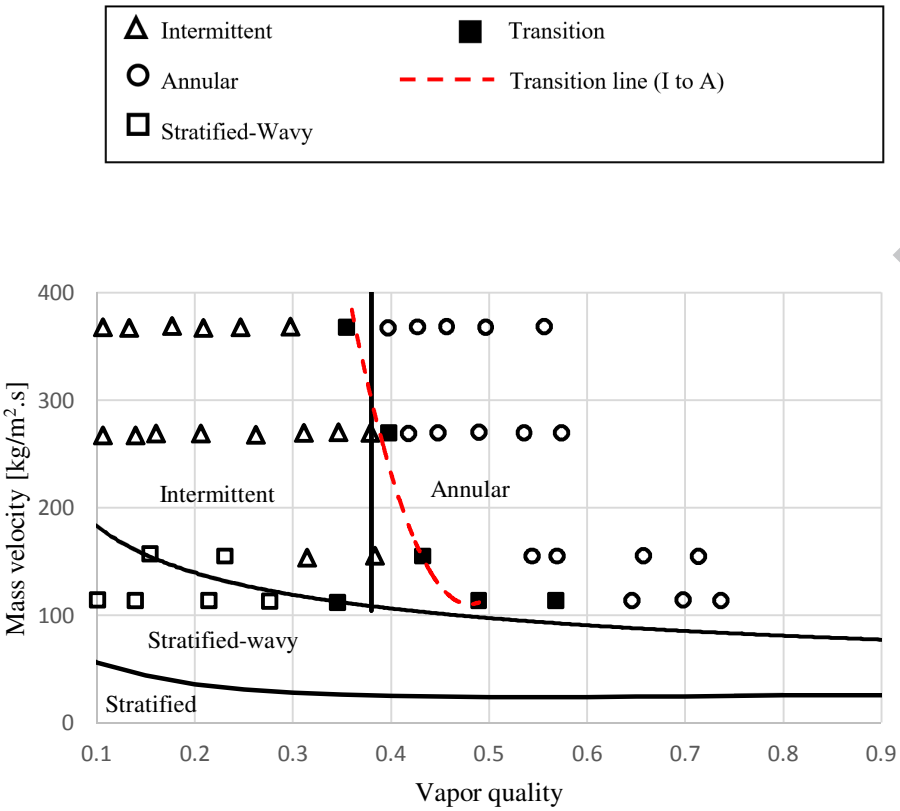

Fig. 6. Comparison between the observed flow patterns for the smooth tube and the El Hajal et al. [11] map.

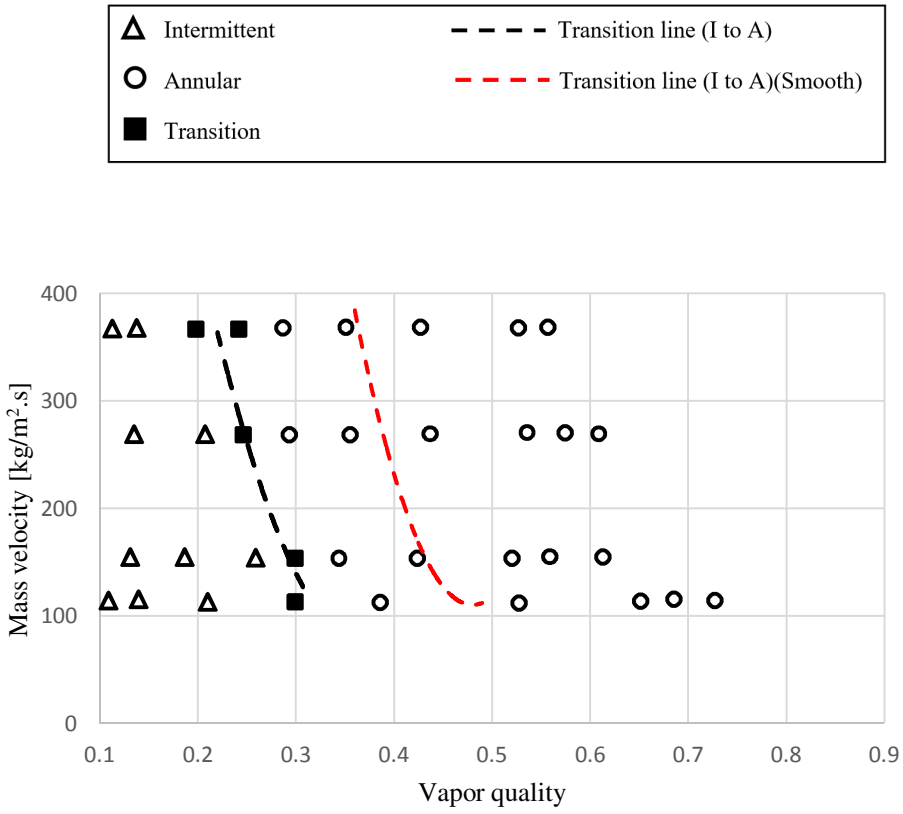

Fig. 7. Observed flow patterns for the helically dimpled tube. Data are reported using the coordinates of the El Hajal et al. [11] map.

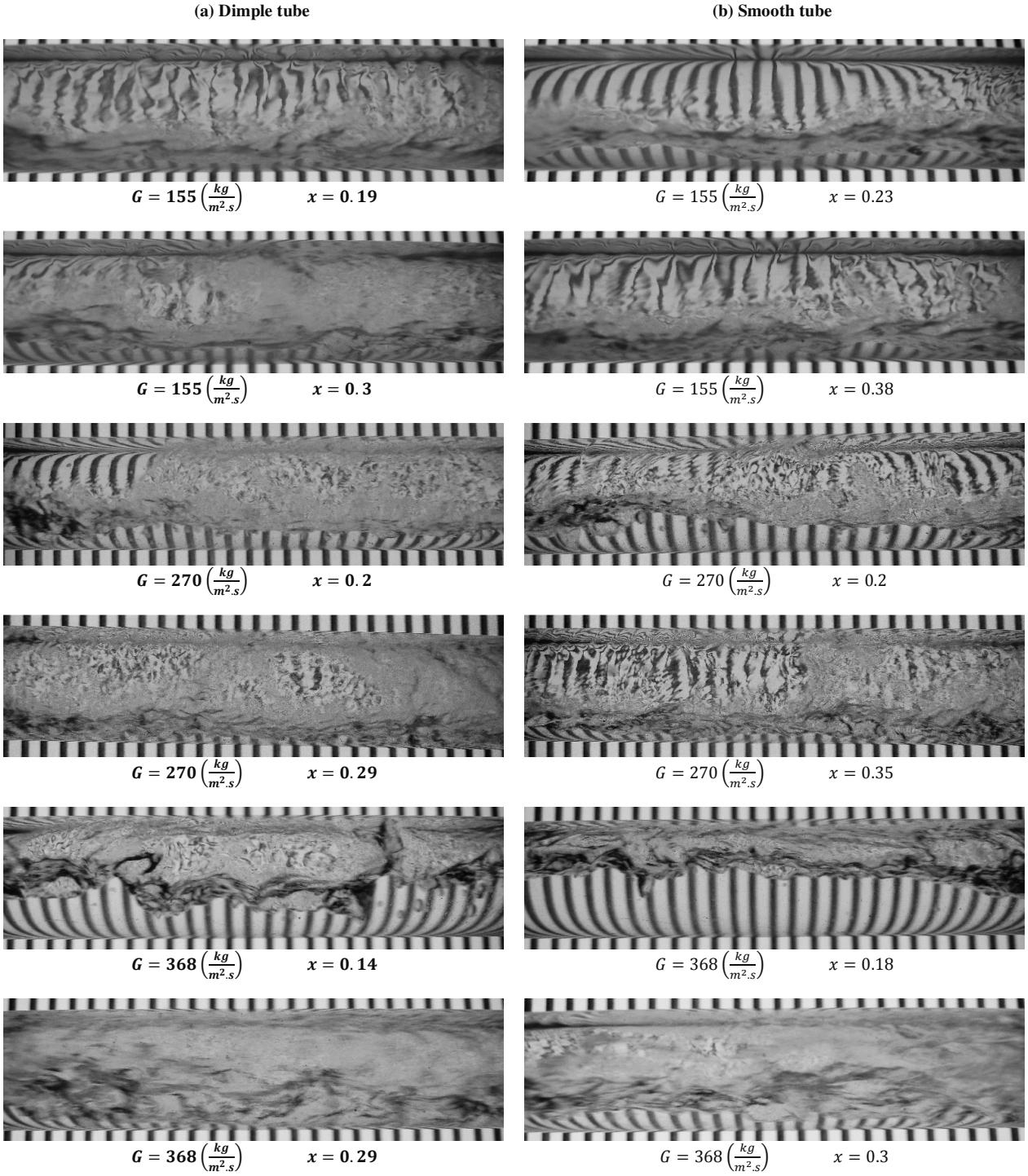

Fig. 8. Two-phase flow patterns for condensation inside a) the helically dimpled tube versus b) plain tube at three mass fluxes of 155 kg m^{-2} s^{-1}, 270 kg m^{-2} s^{-1}, and 368 kg m^{-2} s^{-1} at different vapor qualities.

Highlights

- Dimples in both evaporation and condensation influence the flow patterns.
- Intermittent and annular flows were dominant flow pattern for the dimpled tube.
- There was no stratified-wavy flow in the flow pattern map of the dimpled tube.
- Transition lines of both dimpled and plain tubes were recognized and compared.
- Transitions for the dimpled tube occurred at a lower x than the plain tube.